Available online at www.sciencedirect.com

ScienceDirect

Procedia Manufacturing 34 (2019) 672–677

Procedia MANUFACTURING

www.elsevier.com/locate/procedia

47th SME North American Manufacturing Research Conference, Penn State Behrend Erie, Pennsylvania, 2019

An approach to improve interface healing in FFF-3D printed Ultem 1010 using laser pre-deposition heating

Pu Han, Alireza Tofangchi, Anagh Deshpande, Sihan Zhang, Keng Hsu*

J. B. Speed School of Engineering. University of Louisville, Louisville, USA

* Corresponding author. Tel.: 502-852-8616; fax: 502-852-8616. *E-mail address:* Keng.Hsu@louisville.edu

Abstract

Fused Filament Fabrication (FFF) 3D printing has become an effective way to fabricate custom parts at low cost and fast speed. However, due to anisotropic properties of FFF 3D printed parts, their mechanical strength is unsatisfactory compared to those of parts made using traditional methods. To address this issue, an in-process laser local pre-deposition heating (LLPH) method is reported to increase thermal relaxation at inter-layer interface, for improvement of inter-layer adhesion, and therefore tensile strength in the build direction. The effect of laser power on tensile strength, and in-depth investigation of polymer relaxation, reptation and entanglement are presented. 178% increase in tensile strength and an isotropy value of 82.8% (build-direction strength divided by build-plane strength) were achieved. Isotropic behavior at inter-layer interface was observed using Scanning Electron Microscope.

Keywords: 3D printing ; Additive Manufacturing ; Fused Deposition Modeling ; Inter-layer bond ; Inter-layer strength

1. Introduction

Fused filament fabrication (FFF) has become the preferred method for additive manufacturing of polymers because of its flexibility and cost-effectiveness [1]. The process uses thermoplastic filaments as starting material. The filament is extruded through a heated nozzle, which is maintained above the glass transition temperature of the polymer, and directly deposited to construct a 3D component layer-by-layer [2]. Components with complex shapes can be fabricated easily using slicing software to control process parameters such as density and inner support pattern [3]. Even though FFF has numerous advantages [4] and is capable of printing large number of applicable materials including amorphous polymers like polycarbonate [5], acrylonitrile butadiene styrene [4] and semi-crystalline polymer like poly-lactic acid [6], it suffers from a few drawbacks. For instance, parts fabricated using this method exhibit fairly low mechanical strength compared to those fabricated with traditional methods, particularly in the build direction, and the mechanical properties of FFF-3D printed parts are anisotropic [7].

To address the issue of mechanical property anisotropy in FFF-printed parts, the major thrust in the literature has been to use statistical analysis tools like design of experiments [8–10], Taguchi method [11–14] , fuzzy logic [15] and parameter investigation [16,17] to optimize process parameters like nozzle temperature, raster strategy, layer thickness and air gap control [18–22].The main drawback of these approaches is that they propose a trade-off between different process parameters to achieve maximum inter-layer strength but do not address the fundamental physics that governs the inter-layer bond formation mechanism. Some other approaches to improving mechanical properties of FFF printed components include printing in vacuum to reduce the porosity and heat losses due to conduction [23], printing in low oxygen environment [24] or using a post-processing thermal treatment [25].

The inter-layer strength of FFF components is dependent on the motion of polymer chains across the interface between

10.1016/j.promfg.2019.06.195

layers. This motion of polymer chains, referred to as reptation, is a function of the interface temperature and the time during which the temperature remains above the glass transition temperature of the polymer extrudate [26,27]. To this end, raising print temperature can naturally increase interfacial bond strength due to increase in polymer reptation [28]; however, degradation occurs if temperature exceeds a certain limit [29]. In addition, it is found that weld strength is related to welding time as a function of $t^{1/4}$ until polymer in the weld region is fully entangled [30–34]. Many studies have been focused on melting behavior of polymer diffusion in equilibrium state [35,36], where it was found that transient behavior of the polymer melt also plays an important role in forming of final microstructure. These factors suggest a potentially effective method to improve mechanical strength with introducing heat directly to the inter-layer interface during printing.

In their previous work, authors reported on an in-process laser pre-deposition heating technique with near-infrared laser that was used to heat the interface between current and the previous layers in front of the nozzle to introduce heating directly to the region where reptation is needed. A 77% of increase in bonding toughness (in bending test) compared to that of control samples (samples printed without laser pre-deposition) was reached in FFF-printed ABS material [37,38].

In this work, a similar technique was adapted to use CO_2 infrared laser to assist FFF-3D printing of ULTEM 1010. The tensile strength of horizontal control samples (samples tested along the printed track direction), vertical control sample (samples tested along the build direction), laser pre-deposition heating samples and filament feedstock have been compared. Failures at inter-layer interface and its cross-section have been analyzed. Using these results as well as favorable evidence of improved reptation and entanglement across the interfaces, a scalable approach was developed to build nearly isotropic parts.

2. Experimental

2.1. Sample preparation

A high temperature 3D printing platform (Instamsys Funmat HT) was used for pre-deposition laser heating process implementation. The schematic diagram of the setup is shown in Fig. 1. A 0.4 mm E3D stainless steel nozzle was used for all samples in this work. For all prints, 360 ℃ nozzle temperature, 160 ℃ bed temperature and 90 ℃ environment temperature were maintained. Printer motion was controlled by G-codes generated using Instamsys slicing software. Print parameter settings used are shown in Table 1.

Table 1. List of FDM process parameters.

Parameter	Data
Pattern shown in Fig. 2 (a)	Single wall
Layer height	0.2mm
Extrusion width	1mm
Extrusion temperature	360 ℃
Bed temperature	160 ℃
Environment temperature	90 ℃
Nozzle speed	10 mm/s
Filament diameter	1.75mm
Raft	Yes

Black Ultem 1010 (PEI Ultem 1010 black, 3DXTech, Grand Rapids, USA) was used to print all testing samples. Material properties of this filament are given by 3DXTech, which are shown in table 2. Filament feedstock was placed in an oven at 110 ℃ over night for dehydration before print, then filament was placed into printer chamber with Uline Silica Gel Desiccants which was also dehydrated overnight. The printing of all samples was performed within 3 hours of removing the filament from the oven and the filaments were replaced in the oven immediately after printing to avoid hydration. Furthermore, the humidity in the filament chamber was constantly monitored using a monitor (ThermoPro TP50, ThermoPro, Toronto, Canada) to ensure consistent humidity in all print specimens.

Table 2. Ultem 1010 filament specification.

Parameter	Data
Glass transition temperature	217 ℃
Diameter	1.75 mm (+/- 0.05 mm)
Color	Black
Tensile strength	103 MPa
Recommended Extrude Temperature	370 - 390 ℃
Recommended Bed temperature	120 - 160 ℃
Recommended Print speed	20 – 30 mm/s

A single-wall hollow rectangular box without top and bottom, as shown in Fig. 2 (a) was printed layer by layer on raft, with its length along 45 ° to match the direction of laser as shown in Fig 1. Laser was turned on and kept at 0 % energy level during raft print for warm-up and then incrementally turned up to the set energy level when sample printing started. After printing, samples were removed immediately from the build plate and then cooled down in air. A wire cutter was used to cut front side, the only side that pre-deposition laser heating occurred, off for tensile bar milling. A desktop PCB milling machine from Bantam tools was used to mill samples into tensile bars, as show in Fig. 2 (b). Six tensile bars were acquired from each single-wall box. Shape and size of tensile bars are shown in Fig. 2 (c), thickness for all tensile bars were 0.95 mm with negligible variation.

2.2. Localized laser pre-heating apparatus

As shown in Fig. 1, laser beam was generated by a Synrad laser source. The beam was guided through a coupler, optical fiber (2 meters) and finally was focused to an oval shape spot located 4 mm ahead of the nozzle by a collimator that traveled with the print head (Laser collimator was fixed, so only front wall shown in Figure 2 a was pre-heated by laser). Specifications of parts used are shown in Table 3. In this configuration, the surface of existing layer was heated during printing right before material deposition. All laser components used were specifically designed for a laser of 10.6 μm

wavelength. The absorption rate of Ultem at 10.6 μm is above 94% [39].

Table 3. Specifications of laser parts.

Part	Make	Data
Laser source	Synrad 48-1KAN	10.6 μm, 30W max
Coupler	Laser Component	<1dB
Optical fiber	Polymicro	2 meters, < 1dB/meter
Collimator	Laser Component	F=25.4 mm, 19mm
Focused laser	Oval shape	1.5mm*3mm

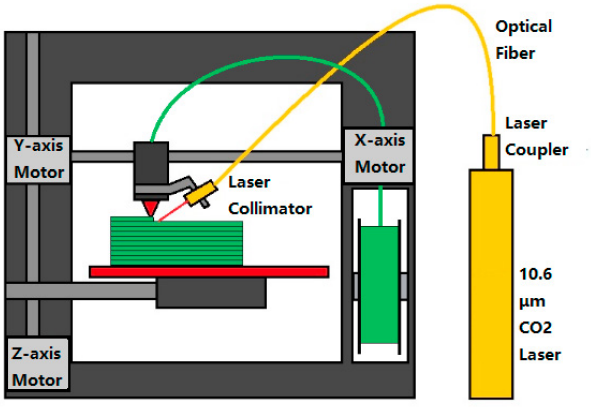

Figure 1. Schematic diagram of experimental set for FFF printing using pre-deposition laser heating.

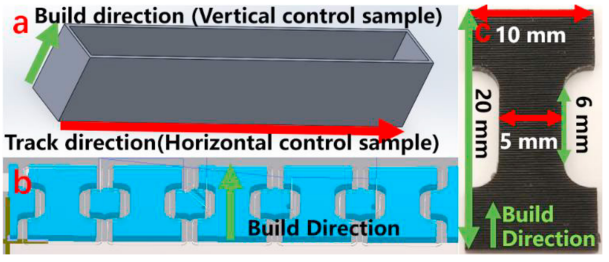

Figure 2. (a) CAD file for single wall rectangular box; (b) G-code for vertical tensile bar milling in Bantam tools software; (c) Machined vertical tensile bar.

2.3. Mechanical testing-tensile strength

A tensile testing machine (MTI-2K, Measurements Technology Inc. Marietta, US) was used to carry out tensile test for all print specimens. 5 samples in each set were examined, the 6th samples in each set was used to remove error samples, such as samples that broke at clip position. Pull speed was set at 3 mm/min for each test specimens. Breaking load (highest load) for all vertical samples, and ultimate tensile strength (highest load in force-deflection curve) for horizontal control samples were used to calculate averages and standard deviations.

3. Result and discussion

Due to the nature of rastering of printed tracks in vertical samples, the net areas consisting physical materials are only 92.1%, 76.9% and 85.7% of the nominal areas measured using a caliper for horizontal control, vertical control and laser-assisted samples respectively. These values were used as correction factors. The tensile strength value of horizontal control samples was used as isotropic reference.

Tensile strength of laser pre-deposition heating samples and two control samples are shown in Fig. 3 where average values and standard deviations are calculated from 5 samples in each set. With laser power ranging from 0.33 W to 2 W, tensile strength of filament feedstock (black line), extruded feedstock (dark green line), vertical control samples (light green line) and horizontal control samples (blue line) are marked as reference lines in the plot for comparison.

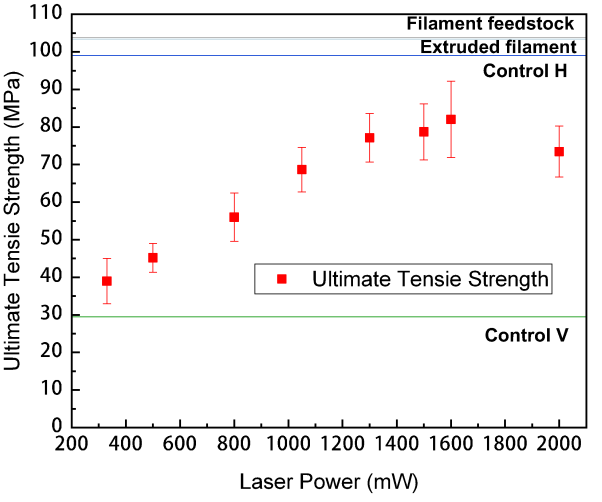

Figure 3. Tensile strength of laser and control samples.

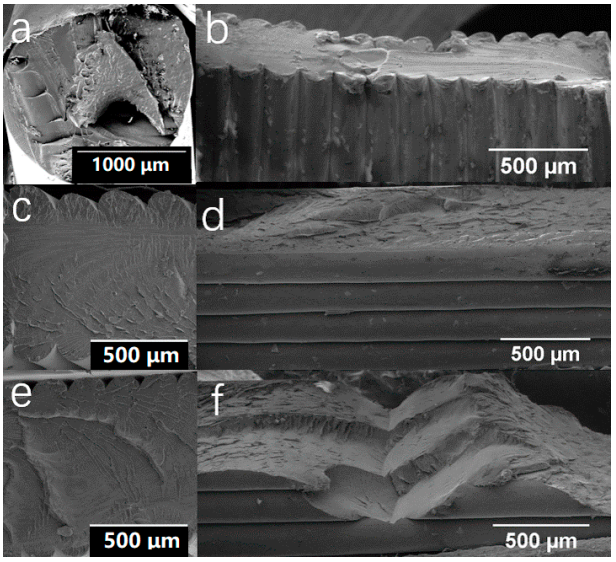

Fig. 4. (a) Cross section of Ultem 1010 filament, (b) Cross section of horizontal control sample break with tensile test; (c) Freeze fracture surface, and (d) tensile test failure surface of vertical control sample (e) Freeze fracture surface and (f) tensile test failure surface of 1.6 W laser sample.

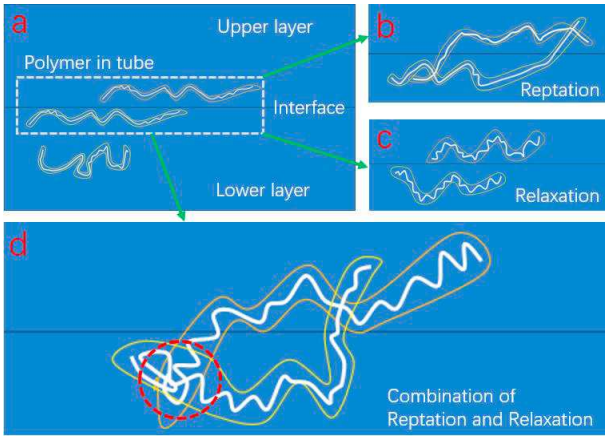

Fig. 5. Schematic diagram of Reptation and Relaxation, (a) polymer in stretched and disentangled status, (b) reptation only, (c) relaxation only, (d) combination of reptation and relaxation, with entangled arear circled in red.

Average tensile strength of filament measured by using the tensile tester machine (MTI-2K) was found to be 103.9 MPa, which is in close agreement with the value of 103 MPa provided by the manufacturer. An SEM image of the cross section of the filament after tensile testing is shown in Fig. 4 (a). The center part of filament shows a very rough fracture surface while the outer edge shows a relatively smoother fracture surface. This disparate fracture morphology in the center and the edges of the filament can be attributed to the difference in the material flow rate between the center and the edge. During extrusion, to make the printing feedstock, the material flow rate at the center is much higher than that at the edge which is closer to the nozzle walls [40]. This results in the polymer chains at the edge being stretched in the direction of extrusion whereas in the center of the extrudate, the polymer chains remain relatively entangled. Thus at onset of fracture, the breakage of polymer chains at the edge of the sample (which are already aligned in the direction of tensile stress) results in a smoother fracture surface than that of the center, where polymer chain are peeled and pulled-out of entangled chains which results in a rougher fracture morphology. When the filament is further extruded from the 0.4 mm printing nozzle diameter without 90° turn, it showed a slightly lower tensile strength of 103.4 MPa. The authors attribute this drop in strength to the reduction of flow path diameter as the polymer melt travels through the nozzle, which leads to further stretching and disentanglement in the extruded filament as opposed to the material in the filament feedstock.

As the polymer flows through the nozzle to a printed track on a horizontal surface, a 90 ° turn in the polymer flow is imposed. This transition alone has been predicted to generate greater amount of stretching and disentanglements [40]. However, the analysis in the referred study was based on the condition where the distance between the nozzle and the print surface is greater than the diameter of the extruded filament, and that the extruded filament lays freely on the print surface (or the pervious layer) with only a slight diameter change. In the print conditions used in this study (and most typical print conditions in general), the extruded polymer melt was squeezed in between the nozzle and print surface to form the printed track height. As a result, more stretching and therefore more strain and disentanglement were created, as shown in Fig. 5 (a). Furthermore, residual stresses along nozzle travel direction can weaken material in this direction and therefore results in only 95.8% of tensile strength of extruded filament in horizontal control samples. Unlike horizontal control samples, whose tensile strength is based on strength along direction of polymer chain, that of vertical control samples is dominated by inter-layer interface reptation and microstructure around interfaces. It is conceivable that the degree of disentanglement and residual stress increases towards the external surface of the extruded filament (due to nozzle flow and 90 ° turn), which should in turn increase the degree of diffusion due to chain alignment in regions near the interfaces. In most typical prints, however, not enough time at high temperature is allowed for interface healing (re-entanglement and relaxation) to occur. Most polymer chains near interfaces, therefore, show microstructure similar to that represented in Fig. 5. (b) (crossed, but not entangled). Thus, the tensile failure in the vertical samples is expected to occur at the inter-layer interface due to lack of entanglement as shown in Fig. 4 (d). As a result, the average tensile strength of vertical control samples was only 29.8% of that in the horizontal control samples without pre-heating.

Laser pre-deposition heating allows higher inter-layer interface temperature, and therefore more reptation and relaxation to happen at the interface, as shown in the conceptual drawing in Fig. 5 (d). Additionally, with the increase of laser power, interface temperature increases further, and more reptation and relaxation can take place. This trend continues until it reaches the degradation temperature (510 ℃) [41] of Ultem where decomposition and generation of local defect occur.

As shown in Fig. 3, the ultimate tensile strength increased with laser power until 1.6 W, where the average tensile strength reached its maximum value at 82.0 MPa, representing 82.8% of strength of the horizontal control sample, and 278% of that of vertical control sample. The decrease of tensile strength at 2 W is attributed to degradation of polymer since burning and smoke were observed during printing at this power level.

The Scanning Electron Microscopy (SEM) images shown in Fig. 4 provide additional insights into the differences in tensile failure. Horizontal control samples shown in Fig. 4 (b) exhibited necking during tensile testing. The authors attribute this observation to the nozzle flow and 90° turn that stretches the polymer cluster which induced residual stress. Since the tensile direction is along the direction of polymer chain alignment, the fracture happens due to breakage of polymer chains resulting in a smoother fracture surface.

For vertical control sample shown in Fig. 4 (d), the mechanical failure happened along the inter-layer interface; in that, the rough fracture surface morphology also shows evidence of polymer chain peeling and pull-out. This also indicates that the interface healing process has gone through reptation (Fig 5. b) at least to some degree. On the other hand, the highly stretched microstructure of polymer chain, as shown in Fig. 5 (b), weakens the inter-layer interface bonding. In fact, although enough time was allowed for reptation to occur between layers to reach its theoretical radius of gyration [42], the polymer chains still remained stretched (Fig. 5 (b)), and hence the inter-layer interface still represented the weakest region. To improve the tensile strength in vertical samples, longer time is needed for both reptation and relaxation (entanglement) to occur and reach to the state shown in Fig. 5 (d).

The laser pre-deposition heating sample (at 1.6 W) shown in Fig. 4 (f) shows fracture trajectories that extends beyond the boundary of the two adjacent layers with an undistinguishable interface. The sample clearly exhibited behavior resembling of isotropic materials. The authors attribute this to the increased temperature and relaxation induced by laser heating which healed the inter-layer interface and the microstructure near interfaces.

The freeze-fracture surfaces of vertical control sample and sample with laser pre-deposition heating can be compared in Fig. 4 (c) and (e) respectively. The control samples show a smoother fracture morphology indicating lesser polymer chain reptation and entanglement. The rougher fracture morphology of the samples printed with pre-deposition heating, again, is attributed to higher reptation and entanglement. Since the sample in (b) is broken by pulling but the sample in (c) is broken by freeze fracture, different fracture behaviors and therefore fracture surfaces geometries and dimensions are expected. Overall, the samples printed with pre-deposition heating exhibited rougher surface morphology. The authors attribute this behavior to the increased temperature-dependent relaxation, which consequently entangled polymer chains and relaxed residual stresses generated through the nozzle flow and 90° turn.

4. Conclusion

In the work presented here, the effect of pre-deposition laser heating process using 10.6 μm laser from 0.33 W to 2 W on the tensile strength and fracture behavior of FFF-printed Ultem 1010 have been investigated. Tensile strength of printed parts in the build direction increased with laser power up to 1.6 W, and reaches 82.8% of that in the print direction (horizontal control sample); equivalent to 178% increase in strength in build direction compared to those in the control samples. This strong inter-layer bonding emerged as a result of increased temperature and time dependent relaxation. It is hypothesized with indirect evidence that the increase in inter-layer strength is due to healing of the interface as a result of higher reptation and entanglement of polymer chains at presence of laser pre-deposition heating. The results markedly highlight the laser pre-deposition heating as a feasible approach to improve the built-part isotropy for the extrusion-based polymer 3D printing processes.

References

[1] Brenken B, Barocio E, Favaloro A, Kunc V, Pipes RB. Fused filament fabrication of fiber-reinforced polymers: A review. Addit Manuf 2018;21:1–16.

[2] Stucker B, Gibson I, Rosen D. Additive Manufacturing Technologies. Springer 2010.

[3] Li L, Sun Q, Bellehumeur C, Gu P. Composite modeling and analysis for fabrication of FDM prototypes with locally controlled properties. J Manuf Process 2002;4:129–41.

[4] N. Turner B, Strong R, A. Gold S. A review of melt extrusion additive manufacturing processes: I. Process design and modeling. Rapid Prototyp J 2014;20:192–204.

[5] Hill N, Haghi M. Deposition direction-dependent failure criteria for fused deposition modeling polycarbonate. Rapid Prototyp J 2014;20:221–7.

[6] Drummer D, Cifuentes-Cuéllar S, Rietzel D. Suitability of PLA/TCP for fused deposition modeling. Rapid Prototyp J 2012;18:500–7.

[7] Ziemian C, Sharma M, Ziemian S. Anisotropic mechanical properties of ABS parts fabricated by fused deposition modelling. Mech. Eng., InTech; 2012.

[8] Horvath D, Noorani R, Mendelson M. Improvement of surface roughness on ABS 400 polymer using design of experiments (DOE). Mater. Sci. Forum, vol. 561, Trans Tech Publ; 2007, p. 2389–92.

[9] Chin Ang K, Fai Leong K, Kai Chua C, Chandrasekaran M. Investigation of the mechanical properties and porosity relationships in fused deposition modelling-fabricated porous structures. Rapid Prototyp J 2006;12:100–5.

[10] Nancharaiah T. Optimization of process parameters in FDM process using design of experiments. Int J Emerg Technol 2011;2:100–2.

[11] Chung Wang C, Lin T-W, Hu S-S. Optimizing the rapid prototyping process by integrating the Taguchi method with the Gray relational analysis. Rapid Prototyp J 2007;13:304–15.

[12] Sood AK, Ohdar RK, Mahapatra SS. Improving dimensional accuracy of fused deposition modelling processed part using grey Taguchi method. Mater Des 2009;30:4243–52.

[13] Zhang JW, Peng AH. Process-parameter optimization for fused deposition modeling based on Taguchi method. Adv. Mater. Res., vol. 538, Trans Tech Publ; 2012, p. 444–7.
[14] Laeng J, Khan ZA, Khu SY. Optimizing flexible behaviour of bow prototype using Taguchi approach. J Appl Sci 2006;6:622–30.
[15] Sahu RK, Mahapatra SS, Sood AK. A study on dimensional accuracy of fused deposition modeling (FDM) processed parts using fuzzy logic. J Manuf Sci Prod 2013;13:183–97.
[16] Sood AK, Ohdar RK, Mahapatra SS. Parametric appraisal of mechanical property of fused deposition modelling processed parts. Mater Des 2010;31:287–95.
[17] Zhang Y, Chou K. A parametric study of part distortions in fused deposition modelling using three-dimensional finite element analysis. Proc Inst Mech Eng Part B J Eng Manuf 2008;222:959–68.
[18] Anitha R, Arunachalam S, Radhakrishnan P. Critical parameters influencing the quality of prototypes in fused deposition modelling. J Mater Process Technol 2001;118:385–8.
[19] Thrimurthulu K, Pandey PM, Reddy NV. Optimum part deposition orientation in fused deposition modeling. Int J Mach Tools Manuf 2004;44:585–94.
[20] Lee BH, Abdullah J, Khan ZA. Optimization of rapid prototyping parameters for production of flexible ABS object. J Mater Process Technol 2005;169:54–61.
[21] Kumar GP, Regalla SP. Optimization of support material and build time in fused deposition modeling (FDM). Appl. Mech. Mater., vol. 110, Trans Tech Publ; 2012, p. 2245–51.
[22] Rayegani F, Onwubolu GC. Fused deposition modelling (FDM) process parameter prediction and optimization using group method for data handling (GMDH) and differential evolution (DE). Int J Adv Manuf Technol 2014;73:509–19.
[23] O'Connor HJ, Dowling DP. Evaluation of the influence of low pressure additive manufacturing processing conditions on printed polymer parts. Addit Manuf 2018;21:404–12.
[24] Lederle F, Meyer F, Brunotte G-P, Kaldun C, Hübner EG. Improved mechanical properties of 3D-printed parts by fused deposition modeling processed under the exclusion of oxygen. Prog Addit Manuf 2016;1:3–7.
[25] Torres J, Cotelo J, Karl J, Gordon AP. Mechanical property optimization of FDM PLA in shear with multiple objectives. Jom 2015;67:1183–93.
[26] Ahn S-H, Montero M, Odell D, Roundy S, Wright PK. Anisotropic material properties of fused deposition modeling ABS. Rapid Prototyp J 2002;8:248–57.
[27] Masood SH, Mau K, Song WQ. Tensile properties of processed FDM polycarbonate material. Mater. Sci. Forum, vol. 654, Trans Tech Publ; 2010, p. 2556–9.
[28] Sun Q, Rizvi GM, Bellehumeur CT, Gu P. Effect of processing conditions on the bonding quality of FDM polymer filaments. Rapid Prototyp J 2008;14:72–80.
[29] Gibson I, Rosen DW, Stucker B. Design for additive manufacturing. Addit. Manuf. Technol., Springer; 2010, p. 299–332.
[30] Jud K, Kausch HH, Williams JG. Fracture mechanics studies of crack healing and welding of polymers. J Mater Sci 1981;16:204–10.
[31] Kline DB, Wool RP. Polymer welding relations investigated by a lap shear joint method. Polym Eng Sci 1988;28:52–7.
[32] Schnell R, Stamm M, Creton C. Mechanical properties of homopolymer interfaces: Transition from simple pullout to crazing with increasing interfacial width. Macromolecules 1999;32:3420–5.
[33] De Gennes P-G. Introduction to polymer dynamics. CUP Archive; 1990.
[34] Ezekoye OA, Lowman CD, Fahey MT, Hulme-Lowe AG. Polymer weld strength predictions using a thermal and polymer chain diffusion analysis. Polym Eng Sci 1998;38:976–91.
[35] Wool RP, O'connor KM. A theory crack healing in polymers. J Appl Phys 1981;52:5953–63.
[36] Ge T, Pierce F, Perahia D, Grest GS, Robbins MO. Molecular dynamics simulations of polymer welding: Strength from interfacial entanglements. Phys Rev Lett 2013;110:98301.
[37] Deshpande A, Ravi A, Kusel S, Churchwell R, Hsu K. Interlayer thermal history modification for interface strength in fused filament fabricated parts. Prog Addit Manuf 2018:1–8.
[38] Ravi AK, Deshpande A, Hsu KH. An in-process laser localized pre-deposition heating approach to inter-layer bond strengthening in extrusion based polymer additive manufacturing. J Manuf Process 2016;24:179–85.
[39] Philipp HR, Le Grand DG, Cole HS, Liu YS. The optical properties of a polyetherimide. Polym Eng Sci 1989;29:1574–8.
[40] McIlroy C, Olmsted PD. Deformation of an amorphous polymer during the fused-filament-fabrication method for additive manufacturing. J Rheol (N Y N Y) 2017;61:379–97.
[41] Carroccio S, Puglisi C, Montaudo G. Thermal degradation mechanisms of polyetherimide investigated by direct pyrolysis mass spectrometry. Macromol Chem Phys 1999;200:2345–55.
[42] McIlroy C, Olmsted PD. Disentanglement effects on welding behaviour of polymer melts during the fused-filament-fabrication method for additive manufacturing. Polymer (Guildf) 2017;123:376–91.